PAPER

Check for updates

Protein corona alleviates adverse biological effects of nanoplastics in breast cancer cells†

Siyao Xiao, [ID] [a] Junbiao Wang, [b] Luca Digiacomo, [a] Augusto Amici, [b] Valentina De Lorenzi, [c] Licia Anna Pugliese, [c] Francesco Cardarelli, [ID] [c] Andrea Cerrato, [d] Aldo Laganà, [d] Lishan Cui, [e,f] Massimiliano Papi, [ID] [e,f] Giulio Caracciolo, [ID] [a] Cristina Marchini*[b] and Daniela Pozzi [ID] *[a]

Pollution from micro- and nanoplastics (MNPs) has long been a topic of concern due to its potential impact on human health. MNPs can circulate through human blood and, thus far, have been found in the lungs, spleen, stomach, liver, kidneys and even in the brain, placenta, and breast milk. While data are already available on the adverse biological effects of pristine MNPs (*e.g.* oxidative stress, inflammation, cytotoxicity, and even cancer induction), no report thus far clarified whether the same effects are modulated by the formation of a protein corona around MNPs. To this end, here we use pristine and human-plasma pre-coated polystyrene (PS) nanoparticles (NPs) and investigate them in cultured breast cancer cells both in terms of internalization and cell biochemical response to the exposure. It is found that pristine NPs tend to stick to the cell membrane and inhibit HER-2-driven signaling pathways, including phosphatidylinositol-3-kinase (PI3K)/protein kinase B (AKT) and mitogen-activated protein kinase (MAPK)/extracellular signal-regulated kinase (ERK) pathways, which are associated with cancer cell survival and growth. By contrast, the formation of a protein corona around the same NPs can promote their uptake by endocytic vesicles and final sequestration within lysosomes. Of note is that such intracellular fate of PS-NPs is associated with mitigation of the biochemical alterations of the phosphorylated AKT (pAKT)/AKT and phosphorylated ERK (pERK)/ERK levels. These findings provide the distribution of NPs in human breast cancer cells, may broaden our understanding of the interactions between NPs and breast cancer cells and underscore the crucial role of the protein corona in modulating the impact of MNPs on human health.

Introduction

In recent years, the pervasive presence of micro- and nanoplastics (MNPs) in our environment has raised concerns about their potential impact on human health. Microplastics are tiny plastic particles measuring less than 5 millimeters in size,[1] while nanoplastics are smaller, with a size in the nanometer range.[2] These particles originate from various sources, including the breakdown of larger plastic debris, microbeads in personal care products, and the degradation of synthetic textiles. The ubiquitous nature of MNPs has led to their widespread distribution in the environment, including air, water, and even food.[3,4] As a result, humans are inevitably exposed to MNPs through ingestion, inhalation, and dermal contact.[5] MNPs were found in different locations in the human body, including the kidneys,[6] lung tissue,[7,8] liver,[9] gastrointestinal tract,[10] placentas,[11] semen[12–15] and even in the bloodstream.[16] Polyethylene (PE), polyethylene terephthalate (PET), polystyrene (PS), polycarbonate (PC) and polyvinyl chloride (PVC) are common plastic types detected in human bodies. Indeed, their small size enables them to circulate through the bloodstream and cross cellular barriers, including the blood–brain barrier,[17] potentially reaching sensitive target sites.[18] Such findings raise concerns about their potential adverse health effects. The potential physical and chemical interactions between MNPs and biological systems are currently under investigation. Preliminary studies focused on gastrointestinal

a NanoDelivery Lab, Department of Molecular Medicine, Sapienza University of Rome, Viale Regina Elena 291, 00161 Rome, Italy. E-mail: daniela.pozzi@uniroma1.it
b School of Biosciences and Veterinary Medicine, University of Camerino, 62032 Camerino, Italy. E-mail: cristina.marchini@unicam.it
c Laboratorio NEST, Scuola Normale Superiore, Piazza San Silvestro 12, 56127 Pisa, Italy
d Department of Chemistry, Sapienza University of Rome, P.le A. Moro 5, 00185 Rome, Italy
e Department of Neuroscience, Catholic University of the Sacred Heart, Largo Francesco Vito 1, Rome 00168, Italy
f Fondazione Policlinico Universitario A. Gemelli IRCSS, Rome 00168, Italy
†Electronic supplementary information (ESI) available. See DOI: https://doi.org/10.1039/d4nr01850h

cell models have suggested that MNPs may induce oxidative stress and inflammation finally disrupting cellular function.[19,20] These effects could have long-term consequences on human health, potentially contributing to the development of various diseases, including certain types of cancer.[21] With regard to cancer in particular, Rosenberg and collaborators pointed out that MNPs containing harmful endocrine-disrupting chemicals are able to mimic estrogen exposure, causing changes in breast development that increase the risk of breast cancer later in life.[22] Additional studies have suggested that MNPs can promote metastatic features in human breast cancer cells[23] and can induce resistance to therapeutics in HER2-positive cancers.[24] Finally, it was recently reported that 75% of the breast milk samples taken from 34 healthy mothers were positive for the presence of MNPs,[11] suggesting that the breast tissue might be a sensitive target site for MNP accumulation *in vivo*. We are tempted to assume that, before accumulation at the target site (*i.e.* breast tissue), MNPs get modified upon contact with biological fluids, such as blood or interstitial fluid. In fact, MNPs are expected to rapidly acquire a coating of biomolecules known as the protein corona,[25] a dynamic layer formed by proteins and other biomolecules on the surface of the plastic particles. In general, the protein corona can alter the physicochemical properties of nanoparticles[26] and act as a biological interface, modulating the intracellular trafficking and subsequent biological responses.[27,28] Studies have suggested that the protein corona can provide a protective coating and mitigate cytotoxicity, but in some cases, it may enhance toxicity by increased occurrences of cell interactions.[29,30] Therefore, the primary aim of the present study is to investigate the interactions between MNPs and breast cancer cells and the influence of the protein corona on these interactions. To this end, we utilized commercial models of both cationic polystyrene (PS) NPs and anionic PS NPs, which are commonly detected in the environment, are considered to be relevant to human exposure[31,32] and greatly contributed to significant advances in this research area.[33] Pristine or human plasma pre-coated PS NPs were characterized and then administered to SK-BR-3 cells, an *in vitro* model for HER2-positive breast cancer, followed by systematic tests. Our results suggested the contribution of surface charge on the toxicity of NPs and revealed the influence of NPs on oncogenic pathways. Additionally, we uncovered the role of the protein corona in mediating the effects of NPs on breast cancer cells. Considering that SK-BR-3 cell proliferation and survival mainly rely on HER2 signaling pathways, we studied the effects of coronated PS-NH$_2$ in comparison with pristine PS-NH$_2$ on the two major pathways downstream of the HER2 tyrosine kinase receptor, *i.e.* the MAPK and the PI3K/AKT pathways. AKT is a serine/threonine protein kinase, which regulates a variety of cellular processes including survival, proliferation, and metabolism. Maximal AKT activity is dependent on the phosphorylation status of both Thr308 and Ser473 residues.[34] The MAPK pathways involve a series of protein kinase cascades. Among them, the Raf-MEK-ERK pathway, activated by tyrosine kinase receptors, represents one of the best character-

ized and plays a crucial role in the regulation of cell proliferation. Indeed, once activated by upstream kinases, ERK1 and ERK2 translocate to the nucleus and transactivate transcription factors, changing gene expression programs and promoting cell mitosis.[35] In the newly emerging field of MNPs, there remains much unknown about their impacts on human health, especially MNPs accumulated in breast cancer tissues. The reported findings may expand our understanding of their potential risks and underline the critical importance of considering the protein corona when assessing the impacts of MNPs on human health.

Materials and methods

Sample preparation

The 0.1 μm unmodified-polystyrene (PS, #43302) and amine-modified-polystyrene (PS-NH$_2$, #L9904) beads were purchased from Merck Life Science S.r.l. (Sigma-Aldrich, Milan, Italy). These beads were spherical and provided in aqueous solutions composed of polymer particles at two different concentrations: 10% or 2.5% with water. It is worth mentioning that PS-NH$_2$ particles were labeled with an orange, fluorescent dye (excitation/emission 481/644 nm). Prior to the formation of the protein corona, the PS solutions were diluted in distilled water to reach a concentration of 1 mg mL^{-1} and incubated at 37 °C for 1 hour with human plasma (HP) at the following percentages (v/v): 5%, 10%, 20%, 30%, and 50% to form protein corona on the PS particles.

Size and zeta potential measurements

The hydrodynamic size, polydispersity index (PDI), and zeta potential of the protein-coated PS complexes were measured at room temperature using a Zetasizer Ultra Red (ZSU3305, Malvern Panalytical, UK). The results are presented as the mean ± standard deviation of three independent measurements.

Protein corona isolation

The coronated systems underwent four rounds of centrifugation to isolate the protein-coated PS complexes from excessive HP. The initial centrifugation step removed unbound and loosely bound proteins, while the three subsequent wash steps aimed to fully eliminate any remaining loosely bound proteins.

BCA assay

After protein corona formation, and isolation by centrifugation, the pellets were resuspended in 60 μL of distilled water, and 10 μL of each sample was pipetted into a well of a 96-well plate in triplicate. 200 μL of BCA protein assay reagent was added to each well, and after a 37 °C incubation for 30 minutes, the absorbance was measured at 560 nm using a Glomax Discover System (Promega, Madison, WI, USA). The protein concentration was calculated using a bovine serum albumin (Merck, Germany) calibration curve.

1D SDS-PAGE experiments

After protein corona formation and isolation by centrifugation, the resulting pellets were collected and treated with 1× Laemmli loading buffer and heated at 100 °C for 10 minutes to detach tightly bound proteins from the PS. The samples were then centrifuged again, and the supernatant was collected and loaded onto a gradient polyacrylamide gel (4–20% TGX precast gels, Bio-Rad). The gel was run at 100 V, and the gel image was captured using a ChemiDoc™ Gel Imaging System (Bio-Rad, Hercules, CA, United States) and analyzed using MATLAB (MathWorks, Natick, MA, United States). To eliminate the potential biases caused by protein precipitation, a negative control was employed where pure HP at 50% (*i.e.*, incubated with distilled water) underwent the same experimental procedures.

Nano-liquid chromatography tandem mass spectrometry

For mass spectrometry analysis, all chemicals, reagents and organic solvents were purchased from Merck Life Science (Darmstadt, Germany), unless otherwise stated. Trifluoroacetic acid (TFA) was supplied by Romil Ltd (Cambridge). Bond elut C18 EWP cartridges (50 mg) were purchased from Agilent (Santa Clara, USA), and trypsin was purchased from Promega (Madison, WI, USA). Protein pellets were prepared as reported in previous works.[36] Protein samples were prepared for mass spectrometry analysis through a series of steps. First, they were dissolved in a buffer containing a high concentration of urea (8 mol L^{-1}) and tris(hydroxymethyl)aminomethane hydrochloride (Tris-HCl) buffer (50 mmol L^{-1}, pH 7.8) to facilitate protein unfolding and accessibility. Following complete solubilization, the samples underwent reduction with dithiothreitol (DTT) to break disulfide bonds that could hinder mass spectrometry analysis. Subsequently, alkylation with iodoacetamide modified free cysteine residues in the proteins, preventing unwanted interactions during later stages. The harshness of the solution was then reduced by diluting the urea concentration to 1 mol L^{-1} with additional Tris-HCl buffer. Next, the proteins were digested overnight at 37 °C with trypsin (2 μg), to cleave proteins into smaller peptides suitable for mass spectrometry. The enzymatic reaction was stopped by adding trifluoroacetic acid (TFA) to lower the pH, followed by purification of the resulting peptide mixture using solid-phase extraction cartridges. Finally, the purified peptides were dried and dissolved in a weak solution of formic acid (0.1%) for further mass spectrometry analysis. Peptide samples were analysed by nanoHPLC-MS/MS on an Ultimate 3000 nanoHPLC system coupled to Orbitrap Elite (Thermo Scientific). All the details have been previously described.[37] For each sample, two technical replicates were performed, and then the acquired raw MS/MS data files from Xcalibur software (version 2.2 SP1.48, Thermo Fisher Scientific) were searched against the Swiss-Prot human database by MaxQuant search engine (v1.6.3.4)[38] with the automatic setting for tryptic peptide matching and label free analysis. Protein identification was accepted with at least one unique razor peptide for the protein group and the false discovery rate was set at 0.01 for the identification of peptide-spectrum matches, peptides and proteins. For data analysis, the MaxQuant output "proteinGroups.txt" was used.

Fourier-transform infrared spectroscopy (FTIR) experiments

Coronated PS and coronated PS-NH$_2$ pellets were isolated and purified as mentioned above, and then the pellets were resuspended in 200 μL distilled water. HP, PS, PS-NH$_2$, coronated PS, and coronated PS-NH$_2$ were analyzed using an ALPHA II compact Fourier-transform infrared spectroscopy (FTIR) spectrometer (Bruker), equipped with an attenuated total reflection (ATR) module (Eco-ATR). Specifically for each measurement, 10 μL of the sample suspension was air-dried with a gentle nitrogen stream on a high-throughput ZnSe crystal. Each sample was measured three times. All IR spectra were acquired in the wavelength range of 4000 to 600 cm^{-1}, and for each spectrum, 24 scans at a resolution of 4 cm^{-1} were averaged. The background was acquired before the measurements and then subtracted from each sample spectra. The spectra were registered and preprocessed using the commercial OPUS 8.5 SP1 software, dedicated to the analysis of IR spectral data. Data were then exported and further analyzed with MATLAB.

Cell culture

Two cell lines – breast cancer SK-BR-3 (ER-/HER2+) cells and NIH3T3 fibroblasts – were purchased from the American Type Culture Collection (Rockville, MD). Both cell lines were cultured in Dulbecco's modified Eagle's medium (DMEM, supplied by Gibco, Life Technologies, Carlsbad, CA, USA), fortified with 10% fetal bovine serum (FBS) and 1% penicillin–streptomycin (Gibco, Life Technologies, USA) and maintained at 37 °C with 5% CO$_2$, under a humidified atmosphere.

MTT assay

SK-BR-3 cells were seeded in 96-well plates at a density of 10 000 cells per well and allowed to stabilize for 24 hours in an incubator. Subsequently, the cells were treated with various concentrations of PS particles (ranging from 12.5 to 200 μg mL^{-1}, obtained by serially diluting a previously prepared 2 mg mL^{-1} PS sample in DMEM supplemented with 2% FBS and 1% penicillin–streptomycin) for 72 hours. The MTT assay was used to assess the viability of SK-BR-3 cells. Briefly, 10 μL of MTT was added to the plates and further incubated for 4 hours. Following incubation, the MTT solution was aspirated, and the plates were washed with PBS. Subsequently, 100 μL of DMSO (obtained from Sigma-Aldrich) was added to each well to dissolve the formazan crystals. Finally, the absorbance was measured at a wavelength of 540 nm using a Multiskan Ascent 96/384 Plate Reader. Based on the results, 200 μg mL^{-1} PS and 12.5 μg mL^{-1} PS-NH$_2$ were selected for co-culture with various percentages (ranging from 5% to 50%) of human plasma (HP) to explore the impact of protein corona on nanoplastics toxicity. All results represent the average of at

least three independent experiments and are expressed as the mean ± standard deviation.

Flow cytometry analysis

SK-BR-3 cells were seeded at a density of 5×10^5 cells per well in a 6-well plate and incubated overnight at 37 °C with 5% CO_2. The day after, the medium was removed, and the cells were washed with PBS. Then, DMEM supplemented with 2% FBS was added, and the cells were challenged with 12.5 μg mL^{-1} PS-NH$_2$ or their protein-coated form for 4 h at 37 °C. After 4 h, the cells were washed with PBS to remove free particles and visualized under a fluorescence microscope (Carl Zeiss GmbH, Munich, Germany). After ensuring that all PS-NH$_2$ NPs free in the medium were removed, the cells were collected using trypsin–EDTA, and the pellet collected following centrifugation was suspended in PBS for flow cytometry (BD FACSCalibur, BD Life Sciences, San Jose, CA, USA) measurements. Cells were excited at 488 nm and the emission was detected in an FL1 channel (band-pass filter 530/30 nm). This experiment was performed twice as independent experiments, and within each experiment, the cells were seeded in quadruplicate for each condition, all results are provided in the ESI.†

Confocal fluorescence microscopy analysis

Live-cell fluorescence imaging was carried out using a Zeiss LSM 800 confocal microscope (Jena, Germany) equipped with a 63×, 1.4 N.A. oil immersion objective and GaAsP detectors, with a pinhole aperture set at 1 Airy. Approximately 5×10^4 SK-BR-3 cells were seeded in an 8-well cover glass multi-well (Sarstedt) 24 h before the experiment. The cells were incubated with 12.5 μg mL^{-1} pristine or protein-coated PS-NH$_2$ NPs for 4 h, washed 3 times with PBS, and then labeled with 0.1 μL of 10 mg mL^{-1} Hoechst 33342 (Thermo Fisher) and 0.2 μL of 5 mg mL^{-1} CellMask™ (Thermo Fisher). The Hoechst stain was excited with a 455 nm laser, CellMask™ was excited with a 640 nm laser, and PS-NH$_2$ was excited with a 488 nm laser, with the emission being collected in the 490–700 nm range. Images of 1024 × 1024 pixels were acquired. The same experiment was carried out using non-cancerous NIH3T3 fibroblasts to verify if the influence of protein corona is specifically related to the breast cancer cell line. Afterwards, to determine the fate of NPs, a colocalization analysis was performed. SK-BR-3 cells were co-incubated with various PS-NH$_2$ forms and 1 μM LysoTracker™ Deep Red for 30 min to label lysosomes. The colocalization level between NPs and lysosomes and Mander' and Pearson's correlation coefficients were calculated using the JaCoP plugin for ImageJ software. The confocal experiments were carried out twice as independent experiments and within an experiment, for each condition, the cells were seeded as a duplicate.

Western blot analysis

The breast cancer cell line SK-BR-3 was treated with 12.5 μg mL^{-1} of PS-NH$_2$ in the presence and absence of HP for 24 h before analysis. Following the treatment, cells were har-

vested and lysed using a radioimmunoprecipitation assay (RIPA) buffer consisting of 0.1% SDS, 1% NP40, and 0.5% CHAPS, which was supplemented with a cocktail of protease inhibitors, including aprotinin, sodium orthovanadate, and phenylmethylsulfonyl fluoride (Sigma-Aldrich, St Louis, MO). The proteins were then quantified using the Bradford assay (Bio-Rad), and aliquots of the resulting whole cell lysate were separated *via* sodium dodecyl sulfate-polyacrylamide gel electrophoresis (SDS-PAGE) and transferred to a polyvinylidene difluoride (PVDF) membrane (Immobilon P, Millipore) using the Criterion™ Blotter (Bio-Rad). After transferring to the membrane, primary antibodies to HER2 (#4290, lot #2), pHER2 (Phospho-HER2/ErbB2 (Tyr1248), #2247, lot #9), ERK (#4695, lot 14), pERK (Phospho-p44/42 MAPK (ERK1/2) (Thr202/Tyr204), #4370, lot #12), Akt (#9272, lot #24), pAKT (Phospho-AKT (Ser473), #9271, lot #13), and β-actin (#2247, lot#9), all from Cell Signaling Technology (1 : 1000), were incubated at 4 °C overnight. In particular, Phospho-HER2/ErbB2 (Tyr1248) antibody detects endogenous levels of HER2 only when phosphorylated at tyrosine 1248; Phospho-p44/42 MAPK (ERK1/2) (Thr202/Tyr204) antibody detects endogenous levels of p44 and p42 MAP kinase (ERK1 and ERK2) when dually phosphorylated at Thr202 and Tyr204 of ERK1 (Thr185 and Tyr187 of ERK2), and singly phosphorylated at Thr202; Phospho-AKT (Ser473) antibody detects endogenous levels of AKT1 only when phosphorylated at Ser473 and also AKT2 and AKT3 when phosphorylated at the corresponding residues. The membranes were washed three times and subsequently incubated with secondary antibodies (Sigma-Aldrich, 1 : 20 000) at room temperature for 1 hour. Target protein bands were detected using an enhanced chemiluminescence solution (LiteAblot PLUS, Euroclone), and images were captured using the Chemidoc MP Imaging System (Bio-Rad, Hercules, CA, USA). Finally, densitometric analysis was performed using the ImageJ software. The re-blot plus strong solution (Millipore) was used to strip the membranes when re-blotting was needed.

Statistical analysis

The GraphPad Prism software (ver. 9.0; LaJolla, CA) was used for figures and statistical analyses. Student's t-test was applied to test the statistical significance of the difference between two groups. One way ANOVA was applied to test the statistical significance among three or more groups, followed by Dunnett's or Tukey's multiple comparison test, as specified in the corresponding captions. Data were expressed as means ± standard deviation.

Results

Characterization of pristine and coronated nanoplastics

Dynamic light scattering (DLS) is a widely used technique for characterizing pristine NPs and changes in their chemical–physical features upon exposure to human plasma (HP). To start, we measured the hydrodynamic diameter and zeta potential of unmodified PS NPs and amine modified PS NPs (*i.e.*

PS-NH$_2$) before incubation with human plasma (HP). Results are summarized in Table 1, a full DLS dataset at three different scattering angles is provided in the ESI, Fig. S1.† Unmodified-PS particles had a hydrodynamic size of 125 ± 2 nm with a polydispersity index (PdI) of 0.016, whereas PS-NH$_2$ particles exhibited similar hydrodynamic size (*i.e.* 112 nm) but slightly larger PdI (*i.e.* 0.118).

Furthermore, unmodified-PS particles exhibited a negative zeta potential equal to −58 mV, whereas PS-NH$_2$ systems displayed a positive zeta potential of 64 mV. Overall, this preliminary characterization indicated that, before exposure to HP, the employed particles were nano-scale objects, monodisperse, with opposite surface charge.

To establish the stability of NPs in the HP solution, we measured changes in the hydrodynamic diameter after 1-hour incubation with varying HP concentrations. We found that the size of unmodified-PS particles increased up to 180 nm, whereas PS-NH$_2$ NPs followed a non-monotonous trend (Fig. 1a). Indeed, the size of PS-NH$_2$ particles increased at low plasma concentration, exhibiting a seven-fold larger size at 5% HP. At higher HP concentrations, PS-NH$_2$ particles exhibited smaller sizes that reached a plateau value of 150 nm. The measured PdI as functions of HP concentration is shown in Fig. 1b. PS-NH$_2$ NPs were always less monodisperse than their unmodified counterparts and exhibited a notably large PdI value at HP = 5%. The peculiar size and PdI trend of NH$_2$-PS NPs at low HP concentrations were ascribable to their instability at the isoelectric point. Indeed, at 5% HP, the zeta potential of NH$_2$-PS NPs was close to 0, and at higher HP amounts, it decreased to negative values (Fig. 1c). When particles are close to the charge neutrality, van der Waals forces dominate the electrostatic repulsion and aggregation processes occur. As a result, the size and PdI of the systems remarkably increase. This trend was not observed for unmodified NPs, whose zeta potential changed from −53 mV (0% HP) to a plateau value of about −20 mV. Globally, the obtained results are consistent with the current literature on the protein corona forming on cationic and anionic particles.[39,40]

Finally, to gain a better understanding of the chemical–physical features of protein-coated PS NPs, with respect to their surface modification and their response to increasing concentrations of HP, we isolated the hard corona and quantified the total protein content by the BCA assay (Fig. 1d). Interestingly, PS-NH$_2$ NPs exhibited a peculiar non-monotonous trend, with a maximum centered at 5% HP. Notably, except for 5% HP, the measured protein amount in the hard corona of the systems was larger for unmodified NPs than for amine-modified particles.
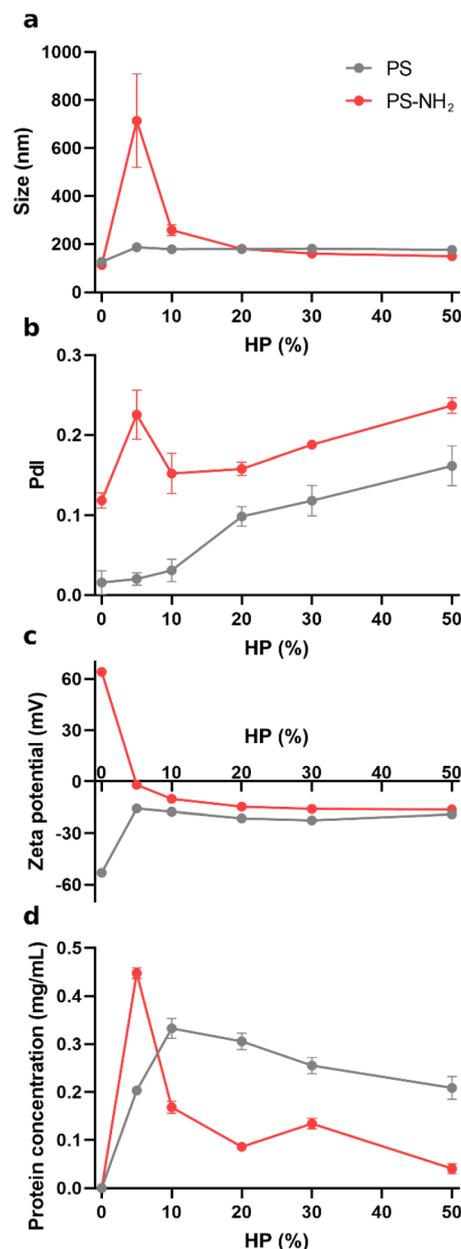

Fig. 1 Characterization of commercial PS and PS-NH$_2$ NPs and their protein-coated counterparts. Hydrodynamic diameter (a), polydisersity (PdI, b), and zeta-potential (c) of unmodified-PS (grey) and PS-NH$_2$ (red) as a function of human plasma (HP) percentage were measured using a Zetasizer. (d) Hard protein corona concentrations at different HP% values were quantified using a BCA assay. Error bars represent mean ± S.D. (*n* = 3).

In summary, this preliminary characterization provided a quantitative analysis of the chemical–physical features of the employed systems, both before and after exposure to HP. The formation of a protein corona on PS NPs and PS-NH$_2$ NPs was confirmed by the BCA assay and had particle-specific effects on the systems' size, PdI, and zeta potential. Protein corona composition was further assessed by 1D SDS-PAGE and mass spectrometry experiments.

Table 1 Hydrodynamic diameter, polydispersity index and zeta potential of pristine unmodified and amine-modified systems

	Size (nm)	PdI	Zeta pot. (mV)
PS	125 ± 2	0.016 ± 0.014	−58.2 ± 1.6
PS-NH$_2$	112 ± 3	0.118 ± 0.010	+64.2 ± 1.1

Protein corona composition

After protein corona formation and isolation, we assessed its composition by 1D SDS-PAGE and nano-liquid chromatography tandem mass spectrometry experiments. Results are shown in Fig. 2. For 1D SDS-PAGE, samples were loaded into a gradient polyacrylamide gel (Fig. 2a), and the corresponding protein corona patterns at different HP concentrations were obtained (Fig. 2b–f). Notably, the lane intensities for PS NPs were larger than the corresponding ones for PS-NH$_2$ NPs, except at 5% HP (Fig. 2a). This trend agrees with the results from BCA and is reported in detail in ESI Fig. S2.† More inter-

estingly, as Fig. 2a and b clearly show, the protein corona composition of unmodified-PS was distinct from that of amine-modified-PS particles, for any of the explored conditions of HP concentrations. Indeed, by analyzing the gel image, we provided a semi-quantitative description of the band intensities. For instance, proteins in the range of 45 kDa to 60 kDa constituted the major component of the protein corona on unmodified-PS. Interestingly, their band intensity decreases significantly on amine-modified-PS, which in turn exhibited a dominant contribution in the range within 22 kDa and 27 kDa. Furthermore, we performed FT-IR spectroscopy to achieve chemical characterization of both pristine NPs and NPs
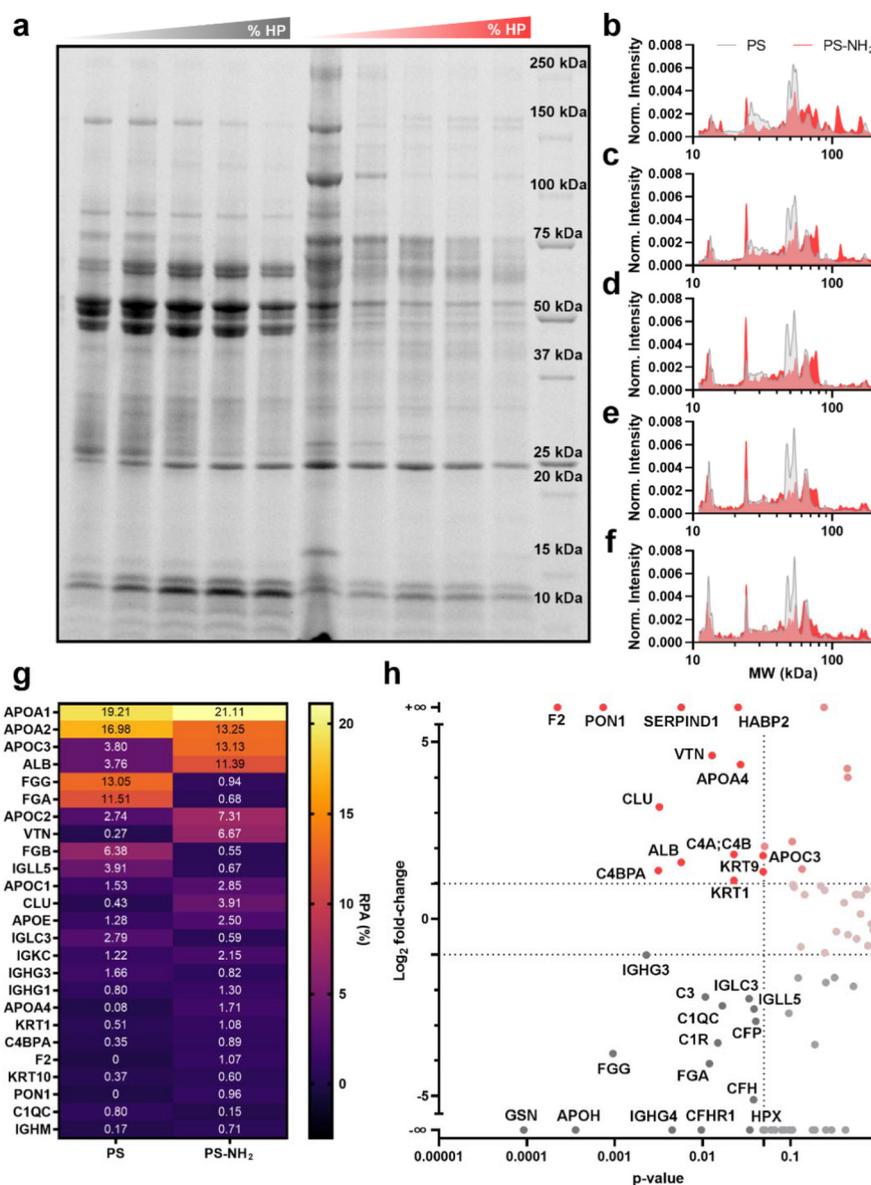

Fig. 2 (a) Gel image and densitometric analysis of the protein corona patterns for unmodified PS NPs and PS–NH$_2$ PS at (b) 5% HP, (c) 10% HP, (d) 20% HP, (e) 30% HP, and (f) 50% HP. (g) Most abundant proteins in the corona of the investigated systems at 30% HP, and (h) the corresponding Volcano plot.

exposed to 30% human plasma (HP), hereafter referred to as coronated NPs. Results are shown in ESI Fig. S3† and clearly indicate that coronated particles exhibit distinct HP signatures in their FT-IR spectra, demonstrating the formation of a protein corona on their surfaces. All the details are provided in the ESI.†

Nano-liquid chromatography tandem mass spectrometry analysis provided the identification of proteins and corresponding abundances in the corona of PS and PS-NH$_2$ systems, at 30% HP. The 25 most abundant proteins are reported in Fig. 2g, and all the identified proteins are listed in ESI Table S1.† The choice of the HP concentration is based on achieving equilibrium in the physical properties (size and zeta-potential) at 30% HP, as well as the significant reduction in toxicity of PS-NH$_2$ at the same concentration (Fig. 3). This latter aspect is detailed in the next section. RPAs of apolipoproteins A1 (APOA1) and A2 (APOA2) were the highest among the identified corona proteins, for both unmodified and amine-modified particles. Furthermore, apolipoprotein A3 (APOA3), albumin (ALB), apolipoprotein C2 (APOC2), and vitronectin (VTN) were remarkably more abundant in the corona of PS-NH$_2$ systems than in that of unmodified PS NPs. However, an opposite and even more prominent trend was found for fibrinogen gamma, alpha, and beta chains (FGG, FGA, and FGB, respectively). To include proteins exhibiting low RPAs, we

proceed by evaluating the RPA fold-change (i.e. RPA in amine-modified NP corona/RPA in unmodified NP corona) and the corresponding p-value by Student's t-test. Results are shown in Fig. 2h, as a Volcano plot. Each dot corresponds to a single protein. Proteins whose RPAs exhibit statistically significant differences populate the left part of the scatter plot and are depicted in red or grey if they are more abundant in PS-NH$_2$ or PS corona, respectively. Shaded dots indicate proteins with less prominent or not-significant differences. Some representative examples of positively-fold-change proteins are clusterin (CLU), albumin (ALB), vitronectin (VTN), and complement proteins C4A, C4B, and C4BPA. In other words, the corona of PS-NH$_2$ systems is more enriched with those proteins than the corona of unmodified particles. Conversely, gelsolin (GSN), beta-2-glycoprotein 1 (APOH), immunoglobulins IGHG3, IGHG4, IGLC3, and IGLL5, complement proteins C3, C1QC, and C1r, complement factors CFH and CFHR1, hemopexin (HPX), and fibrinogen exhibited larger RPAs for unmodified NPs than amine-modified ones.

SK-BR-3 cell viability

We evaluated the viability of SK-BR-3 cells using the MTT assay after 72-hour exposure to unmodified PS and PS-NH$_2$ NPs with identical sizes but different surface charges. At all tested concentrations, unmodified-PS NPs were not toxic, whereas PS-NH$_2$ NPs displayed significant toxicity (Fig. 3a). In detail, at the minimum explored concentration of PS-NH$_2$ NPs (i.e., 12.5 μg mL^{-1}), the cell viability dropped remarkably to 50%. Furthermore, as the doses of PS-NH$_2$ NPs increased, a decreasing trend of cell viability was observed, reaching a plateau value of 20% for NP concentrations ranging from 50 μg mL^{-1} to 200 μg mL^{-1}. Thus, we fixed the NP concentration to the minimum (i.e. 12.5 μg mL^{-1}) and explored the potential effects of the protein corona that formed on NPs upon exposure to increasing HP amounts. Interestingly, a mitigation effect of cytotoxicity was observed for PS-NH$_2$ NPs. Indeed, upon protein corona formation on PS-NH$_2$, we observed an increase of cell viability at increasing HP concentration, until a maximum value of about 70% was reached (Fig. 3b). By contrast, little difference was seen between pristine and protein-coated unmodified PS NPs. Similar cytotoxicity effects were observed on HEK-293 cells. Details can be found in the ESI (Fig. S4†).

SK-BR-3 cellular internalization

We took the advantage of orange fluorescent label on PS-NH$_2$ to assess the internalization of pristine PS-NH$_2$ and protein-coated PS-NH$_2$ NPs at 12.5 μg mL^{-1} by SK-BR-3 cells both quantitatively, using flow cytometry, and qualitatively, using confocal microscopy. Based on our previous results, we fixed the HP percentage to 30%, as under those incubation conditions, the resulting complexes were small, anionic and exhibited intermediate cytotoxicity levels (i.e. cell viability of about 60%). Protein coated PS-NH$_2$ NPs obtained at 30% HP are hereafter referred to as "coronated PS-NH$_2$ NPs". As reported in Fig. 4a and c, flow cytometry experiments revealed
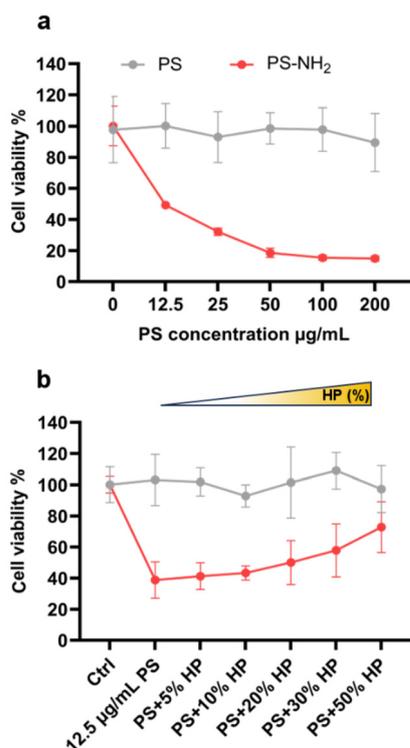

Fig. 3 (a) Cell viability of SK-BR-3 cells upon incubation with PS NPs and PS-NH$_2$ NPs. (b) Cell viability of SK-BR-3 cells upon incubation with coronated PS NPs and PS-NH$_2$ NPs. Results are expressed as the percentage of living cells to untreated cells. Data are reported as mean ± SD, n = 6. Statistical analysis is provided in the ESI, Fig. S5.†
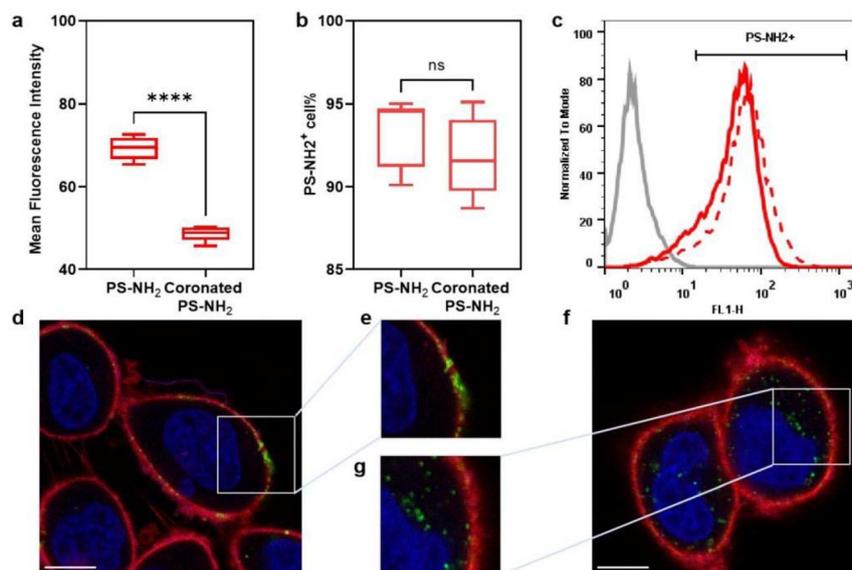
Fig. 4 Cell association and cellular localization of pristine PS-NH$_2$ NPs and coronated PS-NH$_2$ NPs counterparts in SK-BR-3 cells. Cells were exposed to 12.5 μg mL^{-1} pristine particles or coronated particles at the same concentration pre-coated with 30% HP for 4 h, and then the cellular uptake was analyzed by flow cytometry and confocal microscopy. (a) Mean fluorescence intensity, (b) the percentage of positive cells and (c) representative overlayed fluorescence distributions of the control group (grey), PS-NH$_2$ NPs (dashed line) and coronated PS-NH$_2$ NPs (solid line). Data are reported as mean $\pm$ SD, from two independent experiments (in each experiment $n = 4$). * $p < 0.05$; ** $p < 0.01$; **** $p < 0.0001$, as resulted from unpaired Student's t-test. Representative confocal microscopy images of cells treated with pristine PS-NH$_2$ NPs (d and e), and with coronated PS-NH$_2$ NPs (f and g). PS-NH$_2$ particles were shown in green, the plasma membrane in red and the nucleus in blue. Scale bars are 10 μm.

a stronger fluorescent signal for pristine NPs compared to the coronated ones. However, the percentage of PS-NH$_2$+ cells is similar for both the investigated systems (Fig. 4b) and reached 90–95%. These results suggest that while the protein corona reduced the fluorescence intensity of PS-NH$_2$ NPs, it does not affect the cellular uptake of PS-NH$_2$ NPs in SK-BR-3 cells. It is worth noting that flow cytometry cannot differentiate particles adhering to the cell membrane from those that are internalized. Therefore, confocal experiments were performed to verify if protein coating changes the way the NPs interact with cells.

Confocal images revealed clear differences in NP uptake induced by the presence of the protein corona. Specifically, most pristine PS-NH$_2$ NPs (which are in green, commercial fluorescent labeled) tended to stick to the plasma membrane (which is red-stained using CellMask™, as shown in Fig. 4d and e), whereas protein-coated PS-NH$_2$ NPs were significantly more localized in the cytoplasm (Fig. 4g and f), suggesting a major effective uptake in SK-BR-3 cells.

In addition, to understand whether the enhancement of PS-NH$_2$ NPs internalization is specific to SK-BR-3 cells, we employed NIH3T3 fibroblasts for confocal experiments, under the same conditions. The results (Fig. S7 in the ESI†) indicated a similar trend – in which the coronated PS-NH$_2$ NPs were taken up more than pristine PS-NH$_2$ NPs.

Then, we explored the fate of the nanoplastics by quantifying their colocalization with lysosomes. Representative confocal images are shown in Fig. 5a–d where particles are shown

in green, and lysosomes stained using LysoTracker™ Deep Red. Interestingly, PS-NH$_2$ NPs (Fig. 5a and b) colocalized with lysosomes remarkably less than their coronated counterparts (Fig. 5c and d). A quantitative analysis on a dataset containing 20 images was performed in terms of Mander's and Pearson's coefficients. The former is related to the percentage of particles colocalizing with lysosomes, the latter quantifies an overall correlation between the intensities of green and red channels. As reported in Fig. 5e and f, both the parameters reported a significantly higher level of colocalization for coronated systems than for their pristine counterparts. As the lysosomal degradation represents the final step of an intracellular route for objects that are internalized by endocytic mechanisms, taken together our results suggest that the protein corona favored the uptake by endocytosis, delivering the particles to lysosomes and, because of trapping within acidic organelles, lowering cytotoxicity. To investigate the release of the internalized NPs, we also compared the PS-NH$_2$ positive cell percentage 24 hours after the internalization using flow cytometry and observed a significant decrease in the coronated PS-NH$_2$ treated groups; details can be found in ESI Fig. S8.† By contrast, pristine PS-NH$_2$ particles by adhering massively to cell membranes can minimize trapping and degradation while increasing their cytotoxic effects.

The effects on HER-2-driven signaling pathways

At this point, we investigated the signaling pathways in SK-BR-3 cells in response to PS-NH$_2$ NPs. SK-BR-3 cell line
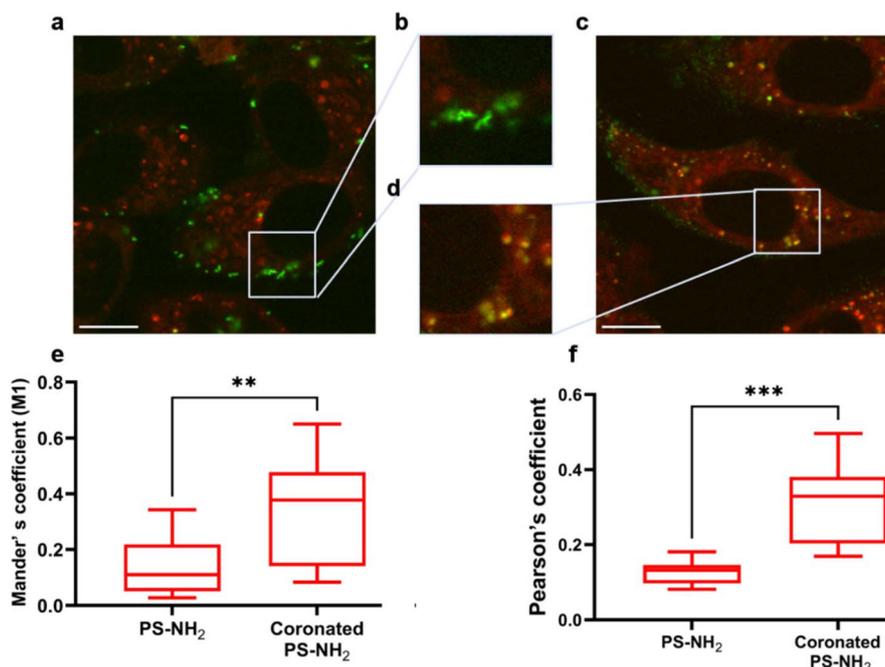
Fig. 5 Colocalization of pristine PS-NH$_2$ NPs and coronated PS-NH$_2$ counterparts with lysosomes. Confocal images of SK-BR-3 cells after treatment with PS-NH$_2$ NPs (green channel) in their pristine forms (a and b) and coronated forms (c and d). Lysosomes were stained in red, scale bars are 10 μm. Quantification of colocalization in terms of (e) Mander's and (f) Pearson's coefficients. Boxplots depict the distributions of measured values over datasets made of $n = 10$ images per group. * $p < 0.05$; ** $p < 0.01$; **** $p < 0.0001$, from unpaired Student's t-test.

serves as an *in vitro* model for HER2-positive breast cancer, characterized by enhanced activation of HER-2-driven signaling pathways, such as phosphatidylinositol-3-kinase (PI3K)/ protein kinase B (AKT) and mitogen-activated protein kinase (MAPK)/extracellular signal-regulated kinase (ERK) pathways, which are linked to cancer cell survival and growth. Interestingly, we neither observed the interference with the HER2 receptor nor the activation (Fig. 6a and b), suggesting that PS-NH$_2$ NPs may not induce its internalization or disrupt receptor dimerization. However, PS-NH$_2$ NPs resulted in a marked decrease in phosphorylated ERK (activated ERK form), and in a slight reduction in pAKT/AKT levels (Fig. 6a, c and d), suggesting that the PS-NH$_2$ NPs might be acting downstream of HER2, directly on components of the ERK and AKT pathways. Notably, the pAKT/AKT and pERK/ERK ratio were restored to control levels in cells treated with coronated PS-NH$_2$ NPs compared to the pristine PS-NH$_2$ NPs treated group. This observation strongly implies that the formation of the protein corona plays a significant role in counteracting the alterations witnessed in cellular signaling pathways caused by PS-NH$_2$ NPs. The protective influence of the protein corona in the restoration of the pAKT/AKT and pERK/ERK ratios to levels comparable to the control group indicates a potential mechanism for toxicity mitigation. This insight underscores the importance of considering the protein corona in understanding and modulating the cellular responses to PS-NH$_2$ NPs, shedding light on a potential mechanism by which nanoplastics interact with and influence cellular signaling networks.

Discussion

The increasing detection of microplastics and nanoplastics in human organs and tissues has raised health concerns. A recent study has confirmed that particles larger than 2.5 μm can enter the digestive system, while those smaller than 1 μm may be transported into the circulatory system and absorbed into different human tissues.[41] However, *in vitro* cell experiments are typically conducted in gastrointestinal cell lines.[42] In this work, we used polystyrene (PS) nanoplastics (NPs) with similar sizes (*i.e.* about 100 nm) but opposite surface charges to study their effects on breast cancer cells. Although these systems represent a simplified model of environmental pollution due to nanoplastics, they are the most employed tools for studying the possible adverse effects of MNPs, both *in vitro* and *in vivo*.[33] Furthermore, the protein corona of similar particles has been previously studied[43] and related to NP behavior in different cell lines.[44,45] Here, we explored the impact of the protein corona on the potential adverse effects of model nanoplastics in breast cancer cells. In agreement with current literature,[39,46] a peculiar trend of size, zeta potential and protein amount was observed for cationic systems exposed to increasing concentration of HP (Fig. 1). This re-entrant condensation phenomenology is typical of cationic systems in mixtures with macromolecules but is generally not observed for anionic particles. Nevertheless, at high HP concentrations (*i.e.* 30% or more), NP–protein complexes exhibited similar chemical–physical features. Despite this similarity, a detailed
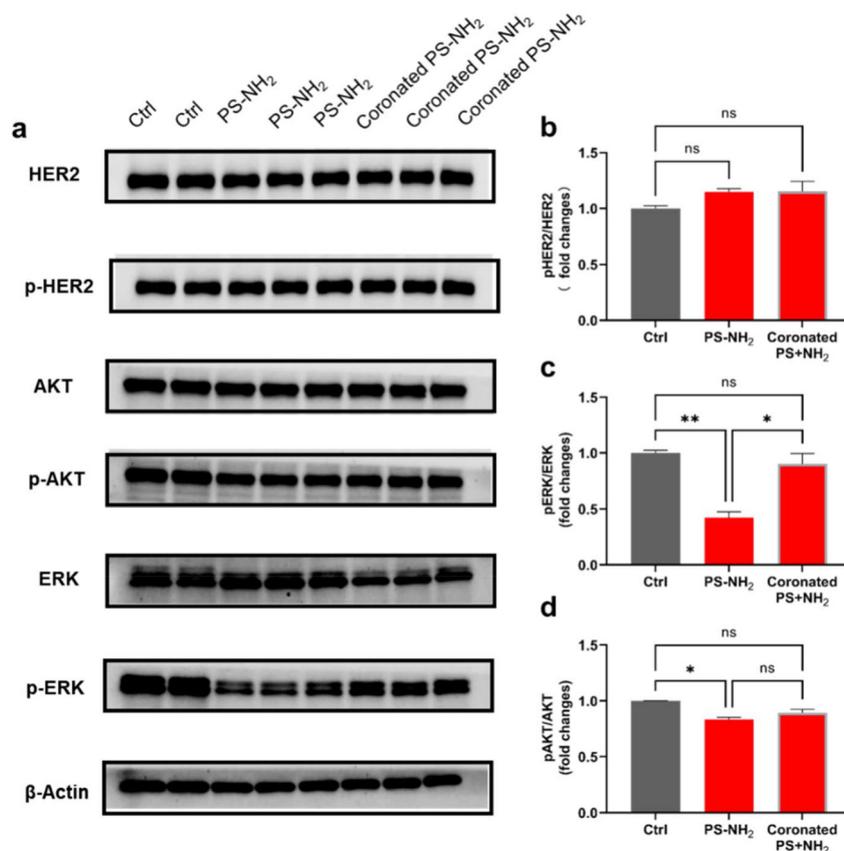
Fig. 6 Different forms of PS-NH$_2$ NPs influence the HER2-driven signaling pathway in different manner. (a) Representative western blot analysis of HER2 downstream signaling pathways in SK-BR-3 cells, treated or not with 12.5 μg mL^{-1} pristine or protein-coated PS-NH$_2$ for 24 h. Expression levels of HER2, pHER2, ERK, pERK, AKT, and pAKT were analyzed. Equal amounts of protein (20 μg) were loaded, and β-actin was used as the loading control. Densitometric quantification of (b) pHER2/HER2, (c) pAKT/AKT, and (d) pERK/ERK are shown. Data are represented as mean ± S.D. (n = 3); one-way ANOVA test followed by Tukey's multiple comparison test (* $p \leq 0.05$; ** $p \leq 0.01$; *** $p \leq 0.001$).

proteomics analysis revealed remarkable differences in their protein corona compositions (Fig. 2). Indeed, although APOA1 and APOA2 were the most abundant proteins in the corona on both systems, APOA3, ALB, APOC2, and VTN were largely more abundant in the corona of PS-NH$_2$, whereas fibrinogen exhibited an opposite trend.

The observed particle-dependent differences reflect the observed behavior of the systems upon interactions with cells. Indeed, we did not observe toxicity of unmodified PS-NPs to SK-BR-3 cells at any of the tested concentrations (from 12.5 to 200 μg mL^{-1}). However, remarkable cytotoxicity was observed for PS-NH$_2$ NPs, and the cell viability decreased to 50% after 48 h of exposure, even at the lowest concentration (Fig. 3). These results are consistent with previous studies on other human cell lines, where they suggested that compared with unmodified PS NPs,[19,47] PS-NH$_2$ NPs increased the cytotoxicity of Caco-2,[48,49] A549 cells,[50] and murine splenic lymphocytes.[51] These results suggested that the cytotoxicity of the NPs was related to their surface charge. In general, positively charged MNPs are more likely to interact with the cell membrane due to the electric attraction; larger MNPs can lead to physical damage, such as perforation or deformation,[52] while NPs

change the permeability of the membrane, generating more ROS[53] and eventually inducing cell apoptosis.[54] Indeed, we did observe a stronger interaction between positively charged PS-NH$_2$ NPs and the cell membrane (Fig. 4). Although we did not observe any altered expression or activation of the membrane receptor (HER2), we detected slight inhibition of AKT activation and remarkable inhibition of ERK activation (Fig. 6), suggesting that the influence on proliferation and survival-related signaling pathways also contributes to the observed cytotoxic effects.

Upon exposure to HP, we observed that the cytotoxicity of the pristine PS-NH$_2$ NPs was altered by the presence of a protein corona, and the cell viability increased to 70% when the PS-NH$_2$ NPs were pre-coated with HP (Fig. 3). These results further confirmed the role of the positive charge on NPs in their toxicity. Similar results have been recently reported.[55]

Given that the unmodified-PS NPs did not exhibit toxicity to breast cancer cells, we proceed with pristine amine-modified systems and their coronated counterparts using the lowest tested concentration, which is 12.5 μg mL^{-1}. It is noteworthy that this concentration falls within the recently reported range of MP concentrations in semen, which is 15.34 ± 23.31 μg

mL^{-1}.[13] We first assessed the degree of internalization using a combination of flow cytometry and confocal microscopy. We found a higher internalization when there was a protein coating on the PS-NH$_2$ NPs. This finding is partially consistent with previous studies. Dietz *et al.* demonstrated that the blood protein corona formation on extracellular vesicles promotes massive uptake by immune cells.[56] However, other studies have suggested that the protein corona can reduce the uptake of nanoparticles in phagocytic cells[57,58] and in lung cancer cells.[59] Contradictory results reported in the literature demonstrate the difficulty in establishing general principles for the interaction between the protein corona and cells. The only undeniable general concept is that nanoparticle interactions with cells are governed by the protein corona, and studies on the biological effects of NPs with the protein corona are still in the initial stage.[60] On the other hand, the mechanism and efficiency of cell internalization and intracellular processing depend specifically on the composition of the protein corona, the exposure of specific conformational epitopes outward, and the coupling between these epitopes and specific receptors of each cell type. In general, it can be concluded that a corona may promote uptake in one cell line and inhibit it in others. Gaining insight into the mechanism governing the interaction between the protein corona and cells, a crucial aspect for predicting the biological response of a nanomaterial necessitates a comprehensive mapping of protein binding sites on the protein corona for each material.[61,62]

Notably, despite their greater internalization in SK-BR-3 cells, coronated nanoplastics show a lower cytotoxicity than their non-coronated counterparts. The colocalization results reported here may explain this effect: following a 4-hour exposure, coronated PS-NH$_2$ NPs are internalized by endocytosis and are readily trapped within lysosomes, while the majority of pristine PS-NH$_2$ NPs mainly located in the cytoplasm. Noteworthy is the fact that several studies have indicated the eventual colocalization of pristine PS-NH$_2$ NPs with lysosomes after prolonged exposure times exceeding 6 hours.[63–65] Nonetheless, because of the chemical stability of plastics, lysosomal enzymes are not able to degrade them effectively,[66] leading to their accumulation in lysosomes and subsequent lysosomal alterations, including the extension of lysosomal volume and intensive lysosomal membrane permeabilization, culminating in lysosome-dependent cell death.[63] On the other side, Han *et al.* have recently demonstrated a separation between NPs and the protein corona within cells, with each entity ending up in distinct morphological compartments.[67] The cellular process directs NPs toward recycling lysosomes, while the protein corona accumulates within multivesicular bodies. The authors infer that NPs undergo preparation for subsequent exocytosis, while the protein corona persists within the cell and undergoes eventual metabolism. In this context, we substituted the exposure medium with fresh PS-NH$_2$ NP-free medium after a 4-hour treatment and measured the proportion of PS-NH$_2$ positive cells 24 hours post medium replacement. In comparison to the PS-NH$_2$ posi-

tive cell ratio at 4 hours, we observed a similar percentage in wells treated with pristine PS-NH$_2$ NPs. Intriguingly, the proportion of PS-NH$_2$ positive cells in wells exposed to coronated NPs decreases markedly, from 92% to 70%, as shown in Fig. S6.† This result suggested that the protein corona on the PS-NH$_2$ NPs may facilitate NP exocytosis or accelerate intracellular NP trafficking, thereby mitigating the cytotoxicity effects.

Given that the protein corona can change the intracellular fate and the final localization of microplastics, we wondered whether the protein corona might influence the effects of PS-NH$_2$ on molecular signaling. Western blot analysis of SK-BR-3 cells revealed that PS-NH$_2$ exposure downregulated the main signaling pathways sustaining cell proliferation and survival, leading to a significant decrease in ERK activation. Of note, the protein corona reversed the effect of PS-NH$_2$ NPs on these signaling pathways, explaining the higher survival rate of cells treated with coronated PS-NH$_2$ than that of cells treated with pristine PS-NH$_2$. Overall, the mitigation effect induced by the protein corona ties well with our previous study in which an HP-coating on graphene oxide (GO) was shown to alleviate the toxicity of GO towards SK-BR-3 cells.[68] Thus, determining the effect of MNPs on human health is essential for evaluating the impact of the protein corona and its influence on MNP interactions with different cell types.

Conclusions

In conclusion, this study enriches the fundamental knowledge regarding the potential impact of micro–nano-plastics on human health. It employed a HER2+ breast cancer model, revealing the possible mechanisms of MNPs' toxicity. Moreover, this work emphasizes the importance of protein corona in the study of nanoplastic–cell interactions. These observations open new and promising avenues for further investigation into the complex interplay among micro- and nanoplastics, biological fluids, and cancer cells and these insights contribute to a deeper understanding of the dynamic relationships between these elements, offering valuable perspectives for advancing research in this arena.

Author contributions

Conceptualization: A. A., F. C., A. L., M. P., G. C., C. M., and D. P.; data curation: S. X., J. W., L. D., L. C., and A. C.; formal analysis: L. D.; funding acquisition: F. C., M. P., G. C., C. M., and D. P.; investigation: S. X., J. W., V. D. L., L. A. P., and L. C.; project administration: C. M. and D. P.; resources: A. A., F. C., G. C., C. M., and D. P.; software: L. D.; supervision: A. A., F. C., M. P., G. C., C. M., and D. P.; validation: S. X., J. W., L. C., A. C., V. D. L., and L. A. P.; visualization: S. X. and L. D.; writing – original draft: S. X.; writing – review & editing: S. X., L. D., F. C., G. C., C. M., and D. P.

Data availability

The data that support the findings of this study are deposited on secure servers at the involved institutions and are available upon reasonable request, subject to institutional approval. Requests with justification can be directed to the corresponding authors to determine if the data can be shared following institutional data access protocols.

Conflicts of interest

There are no conflicts to declare.

Acknowledgements

References

1 J. P. Frias and R. Nash, *Mar. Pollut. Bull.*, 2019, **138**, 145–147.

2 J. Gigault, A. Ter Halle, M. Baudrimont, P.-Y. Pascal, F. Gauffre, T.-L. Phi, H. El Hadri, B. Grassl and S. Reynaud, *Environ. Pollut.*, 2018, **235**, 1030–1034.

3 A. R. Aves, L. E. Revell, S. Gaw, H. Ruffell, A. Schuddeboom, N. E. Wotherspoon, M. LaRue and A. J. McDonald, *Cryosphere*, 2022, **16**, 2127–2145.

4 C. M. Rochman, *Science*, 2018, **360**, 28–29.

5 J. C. Prata, J. P. da Costa, I. Lopes, A. C. Duarte and T. Rocha-Santos, *Sci. Total Environ.*, 2020, **702**, 134455.

6 Y.-L. Wang, Y.-H. Lee, Y.-H. Hsu, I.-J. Chiu, C. C.-Y. Huang, C.-C. Huang, Z.-C. Chia, C.-P. Lee, Y.-F. Lin and H.-W. Chiu, *Environ. Health Perspect.*, 2021, **129**, 057003.

7 L. F. Amato-Lourenço, R. Carvalho-Oliveira, G. R. Júnior, L. dos Santos Galvão, R. A. Ando and T. Mauad, *J. Hazard. Mater.*, 2021, **416**, 126124.

8 L. C. Jenner, J. M. Rotchell, R. T. Bennett, M. Cowen, V. Tentzeris and L. R. Sadofsky, *Sci. Total Environ.*, 2022, **831**, 154907.

9 T. Horvatits, M. Tamminga, B. Liu, M. Sebode, A. Carambia, L. Fischer, K. Püschel, S. Huber and E. K. Fischer, *EBioMedicine*, 2022, **82**, 104147.

10 A. T. Wibowo, H. Nugrahapraja, R. A. Wahyuono, I. Islami, M. H. Haekal, Y. Fardiansyah, P. W. W. Sugiyo, Y. K. Putro, F. N. Fauzia and H. Santoso, *Sustainability*, 2021, **13**, 12840.

11 A. Ragusa, V. Notarstefano, A. Svelato, A. Belloni, G. Gioacchini, C. Blondeel, E. Zucchelli, C. De Luca, S. D'Avino and A. Gulotta, *Polymers*, 2022, **14**, 2700.

12 L. Montano, E. Giorgini, V. Notarstefano, T. Notari, M. Ricciardi, M. Piscopo and O. Motta, *Sci. Total Environ.*, 2023, **901**, 165922.

13 Q. Zhao, L. Zhu, J. Weng, Z. Jin, Y. Cao, H. Jiang and Z. Zhang, *Sci. Total Environ.*, 2023, **877**, 162713.

14 Y. Chen, C. Cheng, W. Xu, Y. Cui, Y. Tian, Y. Jiang, Y. Yuan, R. Qian, Y. Wang and L. Zheng, *Environ. Chem. Lett.*, 2024, 1–7.

15 N. Li, H. Yang, Y. Dong, B. Wei, L. Liang, X. Yun, J. Tian, Y. Zheng, S. Duan and L. Zhang, *Sci. Total Environ.*, 2024, 173522.

16 H. A. Leslie, M. J. Van Velzen, S. H. Brandsma, A. D. Vethaak, J. J. Garcia-Vallejo and M. H. Lamoree, *Environ. Int.*, 2022, **163**, 107199.

17 S. Shan, Y. Zhang, H. Zhao, T. Zeng and X. Zhao, *Chemosphere*, 2022, **298**, 134261.

18 K. Ziani, C.-B. Ioniță-Mîndrican, M. Mititelu, S. M. Neacșu, C. Negrei, E. Moroșan, D. Drăgănescu and O.-T. Preda, *Nutrients*, 2023, **15**, 617.

19 A. Banerjee, L. O. Billey, A. M. McGarvey and W. L. Shelver, *Sci. Total Environ.*, 2022, **836**, 155621.

20 V. Stock, C. Laurisch, J. Franke, M. H. Dönmez, L. Voss, L. Böhmert, A. Braeuning and H. Sieg, *Toxicol. in Vitro*, 2021, **70**, 105021.

21 X. Hu, Q. Yu, M. G. Waigi, W. Ling, C. Qin, J. Wang and Y. Gao, *Environ. Int.*, 2022, **168**, 107459.

22 Cancerwellness mag., TINY PARTICLES, HUGE PROBLEMS, https://cancerwellness.com/.

23 J. H. Park, S. Hong, O.-H. Kim, C.-H. Kim, J. Kim, J.-W. Kim, S. Hong and H. J. Lee, *Sci. Rep.*, 2023, **13**, 6252.

24 H. Kim, J. Zaheer, E.-J. Choi and J. S. Kim, *Theranostics*, 2022, **12**, 3217.

25 A. L. Barrán-Berdón, D. Pozzi, G. Caracciolo, A. L. Capriotti, G. Caruso, C. Cavaliere, A. Riccioli, S. Palchetti and A. Laganà, *Langmuir*, 2013, **29**, 6485–6494.

26 I. Lynch and K. A. Dawson, *Nano Today*, 2008, **3**, 40–47.

27 G. Caracciolo, O. C. Farokhzad and M. Mahmoudi, *Trends Biotechnol.*, 2017, **35**, 257–264.

28 T. Kopac, *Int. J. Biol. Macromol.*, 2021, **169**, 290–301.

29 M. Mahmoudi, M. P. Landry, A. Moore and R. Coreas, *Nat. Rev. Mater.*, 2023, 1–17.

30 M. S.-L. Yee, L.-W. Hii, C. K. Looi, W.-M. Lim, S.-F. Wong, Y.-Y. Kok, B.-K. Tan, C.-Y. Wong and C.-O. Leong, *Nanomaterials*, 2021, **11**, 496.

31 M. Baini, M. C. Fossi, M. Galli, I. Caliani, T. Campani, M. G. Finoia and C. Panti, *Mar. Pollut. Bull.*, 2018, **133**, 543–552.

32 K. E. Goodman, T. Hua and Q.-X. A. Sang, *ACS Omega*, 2022, **7**, 34136–34153.

33 M. T. Ekvall, J. Hua, E. Kelpsiene, M. Lundqvist and T. Cedervall, *Environmental impact of nanoplastics from fragmentized consumer plastics: Final project report*, Naturvårdsverket, 2022.

34 B. D. Manning and L. C. Cantley, *Cell*, 2007, **129**, 1261–1274.

35 W. Zhang and H. T. Liu, *Cell Res.*, 2002, **12**, 9–18.

36 G. Caracciolo, R. Safavi-Sohi, R. Malekzadeh, H. Poustchi, M. Vasighi, R. Z. Chiozzi, A. L. Capriotti, A. Laganà, M. Hajipour and M. Di Domenico, *Nanoscale Horiz.*, 2019, **4**, 1063–1076.

37 G. La Barbera, A. L. Capriotti, C. Cavaliere, F. Ferraris, M. Laus, S. Piovesana, K. Sparnacci and A. Laganà, *Anal. Bioanal. Chem.*, 2018, **410**, 1177–1185.

38 S. Tyanova, T. Temu and J. Cox, *Nat. Protoc.*, 2016, **11**, 2301–2319.

39 F. Giulimondi, L. Digiacomo, D. Pozzi, S. Palchetti, E. Vulpis, A. L. Capriotti, R. Z. Chiozzi, A. Laganà, H. Amenitsch and L. Masuelli, *Nat. Commun.*, 2019, **10**, 3686.

40 R. Cukalevski, S. A. Ferreira, C. J. Dunning, T. Berggård and T. Cedervall, *Nano Res.*, 2015, **8**, 2733–2743.

41 K. E. Carr, S. H. Smyth, M. T. McCullough, J. F. Morris and S. M. Moyes, *Prog. Histochem. Cytochem.*, 2012, **46**, 185–252.

42 R. Gautam, J. Jo, M. Acharya, A. Maharjan, D. Lee, P. B. Kc, C. Kim, K. Kim, H. Kim and Y. Heo, *Sci. Total Environ.*, 2022, **838**, 156089.

43 S. Kihara, S. Ghosh, D. R. McDougall, A. E. Whitten, J. P. Mata, I. Köper and D. J. McGillivray, *Biointerphases*, 2020, **15**, 051002.

44 C. C. Fleischer and C. K. Payne, *Acc. Chem. Res.*, 2014, **47**, 2651–2659.

45 C. C. Fleischer and C. K. Payne, *J. Phys. Chem. B*, 2012, **116**, 8901–8907.

46 F. Giulimondi, E. Vulpis, L. Digiacomo, M. V. Giuli, A. Mancusi, A. L. Capriotti, A. Laganà, A. Cerrato, R. Zenezini Chiozzi, C. Nicoletti, H. Amenitsch, F. Cardarelli, L. Masuelli, R. Bei, I. Screpanti, D. Pozzi, A. Zingoni, S. Checquolo and G. Caracciolo, *ACS Nano*, 2022, **16**, 2088–2100.

47 T. Xia, M. Kovochich, M. Liong, J. I. Zink and A. E. Nel, *ACS Nano*, 2008, **2**, 85–96.

48 M. Busch, G. Bredeck, A. A. Kämpfer and R. P. Schins, *Environ. Res.*, 2021, **193**, 110536.

49 A. P. Walczak, E. Kramer, P. J. Hendriksen, P. Tromp, J. P. Helsper, M. Van Der Zande, I. M. Rietjens and H. Bouwmeester, *Nanotoxicology*, 2015, **9**, 453–461.

50 G. Halimu, Q. Zhang, L. Liu, Z. Zhang, X. Wang, W. Gu, B. Zhang, Y. Dai, H. Zhang and C. Zhang, *J. Hazard. Mater.*, 2022, **430**, 128485.

51 Y. Li, M. Xu, Z. Zhang, G. Halimu, Y. Li, Y. Li, W. Gu, B. Zhang and X. Wang, *J. Hazard. Mater.*, 2022, **424**, 127508.

52 S. Li and N. Malmstadt, *Soft Matter*, 2013, **9**, 4969–4976.

53 X.-D. Sun, X.-Z. Yuan, Y. Jia, L.-J. Feng, F.-P. Zhu, S.-S. Dong, J. Liu, X. Kong, H. Tian and J.-L. Duan, *Nat. Nanotechnol.*, 2020, **15**, 755–760.

54 Q. Ning, D. Wang, J. An, Q. Ding, Z. Huang, Y. Zou, F. Wu and J. You, *J. Hazard. Mater.*, 2022, **422**, 126858.

55 J. Wang, J. Cong, J. Wu, Y. Chen, H. Fan, X. Wang, Z. Duan and L. Wang, *TrAC, Trends Anal. Chem.*, 2023, 117206.

56 L. Dietz, J. Oberländer, A. Mateos-Maroto, J. Schunke, M. Fichter, E. M. Krämer-Albers, K. Landfester and V. Mailänder, *J. Extracell. Vesicles*, 2023, **12**, e12399.

57 Y. Yan, K. T. Gause, M. M. Kamphuis, C.-S. Ang, N. M. O'Brien-Simpson, J. C. Lenzo, E. C. Reynolds, E. C. Nice and F. Caruso, *ACS Nano*, 2013, **7**, 10960–10970.

58 Y. Tan, X. Zhu, D. Wu, E. Song and Y. Song, *Environ. Sci. Technol.*, 2020, **54**, 11485–11493.

59 A. Lesniak, F. Fenaroli, M. P. Monopoli, C. Åberg, K. A. Dawson and A. Salvati, *ACS Nano*, 2012, **6**, 5845–5857.

60 H. Zhang, H. Cheng, Y. Wang, Z. Duan, W. Cui, Y. Shi and L. Qin, *Front. Mar. Sci.*, 2022, **8**, 800782.

61 P. M. Kelly, C. Åberg, E. Polo, A. O'connell, J. Cookman, J. Fallon, Ž. Krpetić and K. A. Dawson, *Nat. Nanotechnol.*, 2015, **10**, 472–479.

62 D. O'connell, F. B. Bombelli, A. Pitek, M. Monopoli, D. Cahill and K. Dawson, *Nanoscale*, 2015, **7**, 15268–15276.

63 F. Wang, A. Salvati and P. Boya, *Open Biol.*, 2018, **8**, 170271.

64 W. Song, L. Popp, J. Yang, A. Kumar, V. S. Gangoli and L. Segatori, *J. Nanobiotechnol.*, 2015, **13**, 1–12.

65 F. Wang, M. G. Bexiga, S. Anguissola, P. Boya, J. C. Simpson, A. Salvati and K. A. Dawson, *Nanoscale*, 2013, **5**, 10868–10876.

66 X. Hua and D. Wang, *Rev. Environ. Contam. Toxicol.*, 2022, **260**, 12.

67 S. Han, R. da Costa Marques, J. Simon, A. Kaltbeitzel, K. Koynov, K. Landfester, V. Mailänder and I. Lieberwirth, *Nat. Commun.*, 2023, **14**, 295.

68 L. Cui, E. Quagliarini, S. Xiao, F. Giulimondi, S. Renzi, L. Digiacomo, G. Caracciolo, J. Wang, A. Amici and C. Marchini, *Nanoscale Adv.*, 2022, **4**, 4009–4015.